

B950CF 高强钢超窄间隙激光焊接头组织对残余应力的影响

张成竹, 陈辉*

西南交通大学材料科学与工程学院焊接研究所, 四川 成都 610031

摘要 超窄间隙激光填丝焊(Ultra-narrow gap laser welding, Ultra-NGLW)是一种先进的厚贝氏体钢焊接技术。通过数值模拟和 X 射线衍射法, 分析了超窄间隙激光填丝焊接头残余应力的分布和变化, 结果表明: 在不同厚度(20, 50, 70 mm)的超窄间隙激光填丝焊接头的表面, 残余应力均呈“W”形分布。利用微型剪切试验, 分析了显微组织对接头残余应力的影响, 熔合线处形成的马氏体脆硬组织使接头形成了“软-硬-软”的夹心组织, 导致接头的应力分布与一般的焊接接头不同, 而多层填丝焊的特殊工艺导致接头中间层的应力增加。

关键词 激光技术; 超窄间隙激光填丝焊接; 残余应力; X 射线衍射法; 微型剪切试验; 高强度贝氏体钢

中图分类号 TN249

文献标志码 A

doi: 10.3788/CJL202148.0602101

1 引言

在船舶、管道、深潜结构等制造过程中, 一般的焊接方法会因为热输入过大, 而产生较大的接头变形和残余应力^[1]。超窄间隙激光焊接(Ultra-NGLW)具有焊接可达性高、热输入低、焊接效率高等优点, 在厚板高强贝氏体钢的焊接中具有巨大的优势^[2]。李俐群等^[3]基于有限元计算软件 MARC, 对 16 mm 厚的高强钢激光填丝多层焊接头的温度场和应力场进行了模拟计算, 研究结果显示, 层间保温能够有效降低接头的冷却速度, 减小激光填丝焊的残余应力, 且多层焊的应力集中在接头的中下部焊道及其热影响区。杨明^[4]研究了厚板焊件的残余应力, 发现焊接接头残余应力的最高值位于距接头浅表层表面 5 mm 左右处。他们的研究均指出, 厚板高强钢接头熔合线处的残余应力值相对于焊缝中心残余应力值都有所下降。

与普通弧焊不同, 在多层填丝焊过程中, 复杂的热过程会使各填充层的微观组织不同, 从而导致各微区的力学性能也不相同^[5]。所以高强钢超窄间隙激光填丝焊接头残余应力的分布与其特殊的微观组

织结构有关。针对超窄间隙激光填丝焊接头复杂的微观结构和极不均匀的接头微区力学性能^[6], 本文通过微型剪切试验, 研究了超窄间隙激光填丝焊接头的微区力学性能与微观结构的关系。权思勇等^[7]采用微型剪切试验, 研究了特大型水电站引水钢管的焊丝筛选, 指出微型剪切试验能够准确地测定焊接接头各狭窄区域内材料的性能以及它们的变化规律, 特别是熔合线附近材料性能的变化梯度。Zhang 等^[8]利用微型剪切试验, 研究了 API-X60 管线钢焊接接头的微剪切强度、微剪切塑性和微剪切韧性等局部力学性能, 并将微型剪切试验结果与拉伸试验、维氏硬度试验等常规试验结果进行了比较, 结果吻合良好。

本文从超窄间隙激光填丝焊接头的不同填充层中, 截取包含焊缝、热影响区、母材的试样^[9]进行微型剪切试验, 试样的尺寸为 1.5 mm × 1.5 mm × 40 mm, 并结合 X 射线衍射法和数值模拟, 分析了超窄间隙激光填丝焊接头的残余应力, 研究了贝氏体钢超窄间隙激光焊接头的微观组织对接头残余应力的影响。

收稿日期: 2020-07-14; 修回日期: 2020-07-29; 录用日期: 2020-08-13

基金项目: 科技部重点研发计划(2016YFB1102100)、四川省重点研发项目(2019YFG0288)

*E-mail: xnrpt@swjtu.edu.cn

2 试验设备及材料

2.1 接头焊接工艺及X射线衍射法测试残余应力

本文采用的B950CF是一种贝氏体高强钢,主要用于水轮机、压力容器等,母材的抗拉强度为

975 MPa。采用的焊丝为西冶新材料有限公司专门为B950CF高强钢研制的直径为1.2 mm的KX-01实芯焊丝,抗拉强度为1050 MPa。母材和焊丝的化学元素(表1)采用火花直读光谱法进行测试。

表1 母材和焊丝的主要化学元素(质量分数,%)

Table 1 Key chemical elements of base material and wire (mass fraction, %)

Material	C	Si	Mn	Cr	Ni	Cu	Ti	V	Al	Fe
B950CF	0.128	0.055	1.06	0.522	1.88	0.294	0.008	0.038	0.047	Bal.
KX-01	0.107	0.500	1.95	0.583	2.99	0.006	0.088	0.010	0.012	Bal.

为了比较不同厚度的超窄间隙激光填丝焊接头的残余应力,本文采用由TRUMP-10002碟式激光器、Fronius自动送丝机、ABB IRB2600机器

人组成的激光填丝焊接装备,对三种不同厚度的超窄间隙激光填丝焊接头(图1)进行了成功焊接。

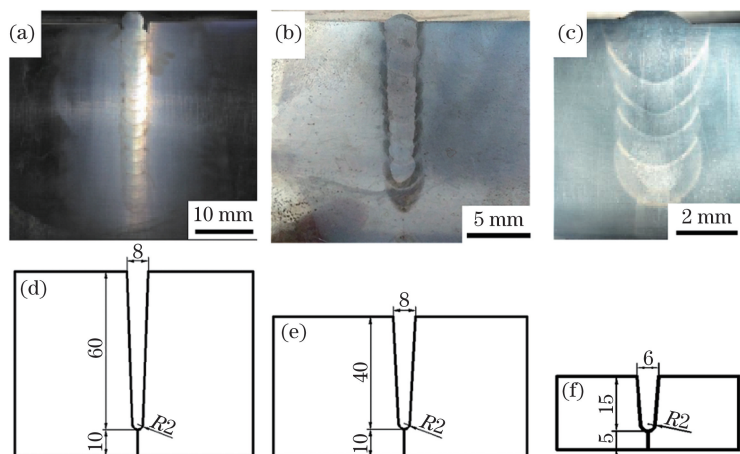


图1 不同厚度超窄间隙激光填丝焊接头及其坡口设计。(a)(d) 70 mm;(b)(e) 50 mm;(c)(f) 20 mm

Fig. 1 Ultra-NGLW joint with each thickness and its groove design. (a)(d) 70 mm; (b)(e) 50 mm; (c)(f) 20 mm

焊接时采用体积分数为20%的CO₂和体积分数为80%的Ar气体作为焊接保护气体。焊接环境控制在20℃和54%湿度。接头钝边采用激光自熔

打底焊接(laser bottoming),超窄间隙坡口采用激光填丝焊接(laser filling),焊接的关键参数如表2所示。

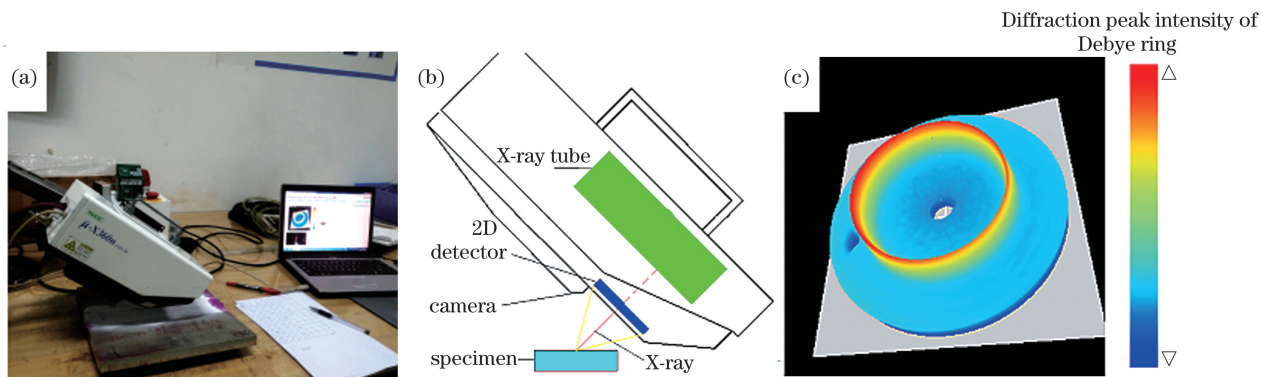
表2 超窄间隙接头激光焊接的关键参数

Table 2 Key parameters for ultra-narrow gap laser welding of joints

Joint thickness	Welding technique	Laser power /kW	Focus /mm	Welding speed / (mm·s ⁻¹)	Feeding speed / (mm·s ⁻¹)
20 mm	Laser bottoming	4.5	0	12	—
	Laser filling	4.0~4.2	12	6.5	5
50 mm	Laser bottoming	8.5	0	12	—
	Laser filling	4.0~4.2	12	6.0~6.2	5.0~5.2
70 mm	Laser bottoming	8.5	0	12	—
	Laser filling	4.0~4.5	12	5.8~6.2	4.8~5.2

采用X射线衍射法对接头的表面残余应力进行测试[图2(a)],残余应力测试示意图如图2(b)所示。设备的相关测试参数如下:采用PultEC实业有限公司的μX360n便携式X射线残余应力测试设

备^[10~11],电压为30 kV,电流为1 mA,工作距离为46 mm,靶材料为αFe(211),射线束入射角为±45°,X射线照射时间为45 s,测试结果以德拜环的形式呈现[图2(c)]。

图2 残余应力测试。(a) μ -X360n 测试设备;(b)测试示意图;(c)德拜环示意图Fig. 2 Residual stress test. (a) μ -X360n test equipment; (b) schematic of test; (c) Debye ring

2.2 数值模拟模型和边界条件

考虑到B950CF的热物理性能和力学性能随温度

的变化规律,用JMat Pro软件对B950CF低合金钢进行材料性能计算,得到的材料热物理性能如表3所示。

表3 B950CF钢的热物理性能参数

Table 3 Thermo-physical performance parameters of B950CF steel

Temperature / ℃	Density / $(\text{kg} \cdot \text{m}^{-3})$	Specific heat capacity / $[\text{J} \cdot (\text{kg} \cdot \text{°C})^{-1}]$	Thermal conductivity / $[\text{W} \cdot (\text{m} \cdot \text{°C})^{-1}]$	Poisson's ratio	Elastic modulus / (10^{10} Pa)	Coefficient of linear expansion / (10^{-5} °C)
25	7870	453	71.98	0.29	212	1.22
400	7760	652	41.17	0.30	185	1.33
600	7680	863	34.08	0.31	160	1.42
800	7680	590	26.19	0.34	128	1.06
1000	7570	623	28.70	0.36	109	1.35
1200	7470	653	31.21	0.36	88	1.54
1400	7360	685	33.72	0.38	67	1.68
1600	6970	821	35.47	0.50	0	2.75

基于ABAQUS模拟软件,建立了70 mm厚板激光焊接的有限元模型,实现了厚板激光焊接过程的有限元模拟。考虑到焊接接头的对称性,建立了70 mm高、60 mm长、60 mm宽的半焊接接头几何模型。焊接区的最小网格尺寸为2 mm×2 mm×0.66 mm,热影响区外的网格尺寸为4 mm×4 mm×

4 mm[图3(a)],试样的初始温度和环境温度设定为25 ℃。在模型边缘下表面,对部分节点施加固定约束,在上表面对部分节点施加竖直方向的约束[图3(b)]。在焊缝对称面施加对称约束。对称面设为绝热边界,另一面设为换热边界[图3(c)],采用导热系数为30 W/(m²·K)的换热边界条件^[12]。

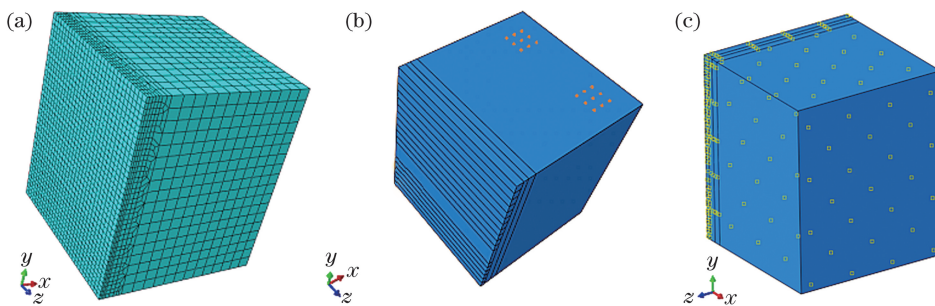


图3 数值模型网格划分与边界条件。(a)网格生成;(b)边界约束条件;(c)换热边界条件

Fig. 3 Meshing and boundary conditions of numerical model. (a) Mesh generation; (b) boundary confinement condition; (c) heat-transfer boundary condition

选择热流沿厚度方向呈线性变化的高斯圆柱热源和高斯热源进行激光打底模拟。在激光填丝焊接过程中,直接选择热流沿厚度方向线性衰减的高斯圆柱热源。高斯圆柱热源表达式为

$$Q_v(r, h) = \frac{6Q_1}{2\pi r_0^2 H + m\pi r_0 H^2} \times \exp\left(-\frac{3r^2}{r_0^2}\right) \times \left(\frac{mh + r_0}{r_0}\right), \quad (1)$$

式中: Q_v 为高斯圆柱热源函数; Q_1 为输入能量; h

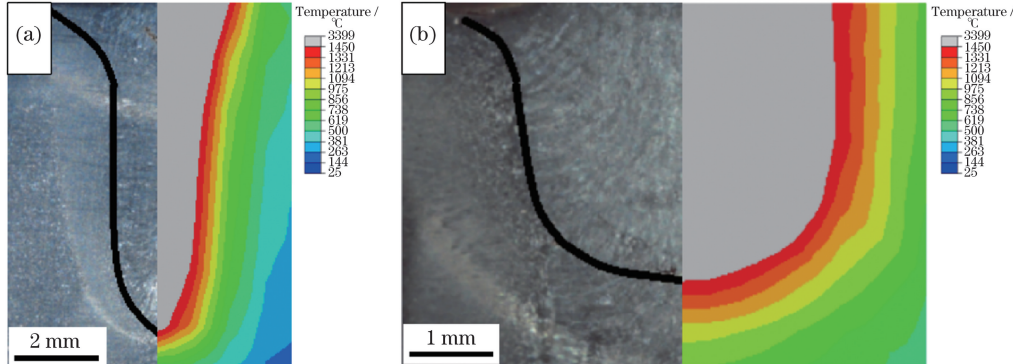


图 4 不同实际熔池与对应热源模型的对比。(a) 激光打底焊熔池;(b) 激光填丝焊熔池

Fig. 4 Comparison of different practical welding pools with their corresponding heat source models. (a) Laser bottoming welded pool; (b) laser filling welded pool

2.3 微型剪切试验

对厚度为 20 mm 的超窄间隙填丝焊接头的第 6 层(表面层, specimen 1)、第 4 层(中间填充层, specimen 2)和第 2 层(底部填充层, specimen 3)取微型剪切试样,试样为 1.5 mm×1.5 mm 的方形截面,长度为 40 mm(图 5)。微型剪切试样涵盖了接头的焊缝区(WM)、热影响区(HAZ)和母材(BM)。用砂纸去除试样表面的污染物和加工痕迹。

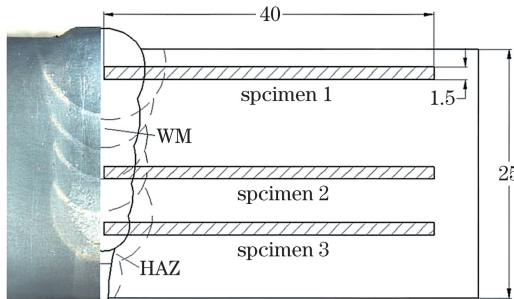


图 5 微型剪切试样取样示意图

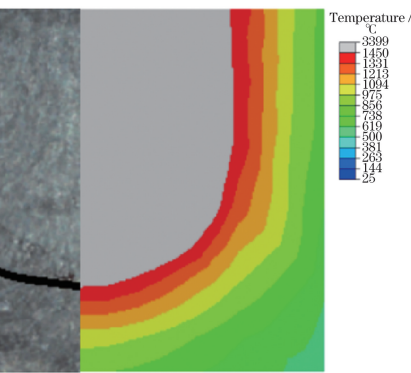
Fig. 5 Schematic for sampling micro-shear specimens

在微型剪切试验中,将截取的试样固定在装置上,该装置能精确控制剪切长度和刀头进给速度,并在刀头装有引伸计,然后对试样进行连续剪切,通过记录剪切的力和位移表征试样的各力学性能。切削头用 WC-Co 硬质合金铣刀[图 6(a)]。每次剪切的

为节点到高斯圆柱热源表面的距离; r 为节点到高斯圆柱热源中心轴的距离; r_0 为热源半径; H 为热源深度; m 为线性衰减系数。高斯热源表达式为

$$Q_s(x, y, z) = \frac{3Q_2}{\pi R_0} \exp\left(-\frac{3x^2 + 3y^2}{R_0^2}\right), \quad (2)$$

式中: Q_s 为高斯热源函数; Q_2 为输入能量; (x, y, z) 为模型的节点坐标; R_0 为表面热源的有效半径。实际熔池截面形貌和热源模型的形貌对比如图 4 所示。



长度为 0.6 mm,刀头进给速度为 1 mm/min^[13]。

载荷与刀具位移之间的关系如图 6(b)所示。微剪切极限强度 τ_b 、拉伸强度 σ_b 以及微剪切韧性 W_t 的表达式分别为

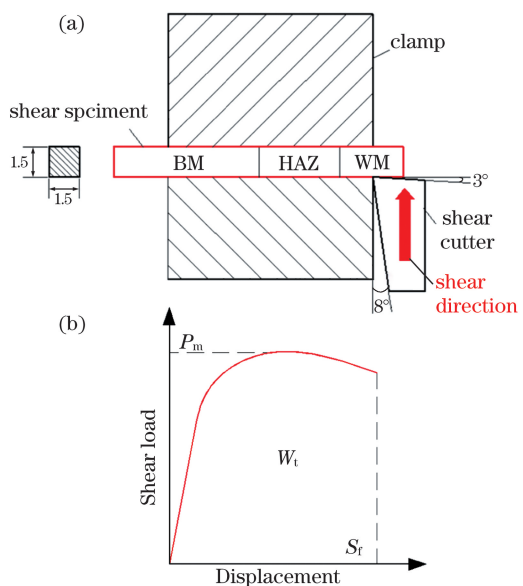


图 6 微型剪切试验。(a)示意图;(b)载荷与刀具位移的关系

Fig. 6 Micro-shear test. (a) Schematic; (b) relationship between load and cutter displacement

$$\tau_b = \frac{P_m}{A_0}, \quad (3)$$

$$\sigma_b = 2.04\tau_b - 227.73, \quad (4)$$

$$W_t = \int_0^{S_f} P(S) dS, \quad (5)$$

式中: P_m 是最大剪切载荷; A_0 是试样的原始横截面积; S_f 是对应试样剪切断裂点的位移; P 为剪切荷载; S 为刀头位移。值得注意的是,(4)式是柏林工业大学基于8种钢材得出的经验公式,用来描述抗拉强度和抗剪强度之间的关系。

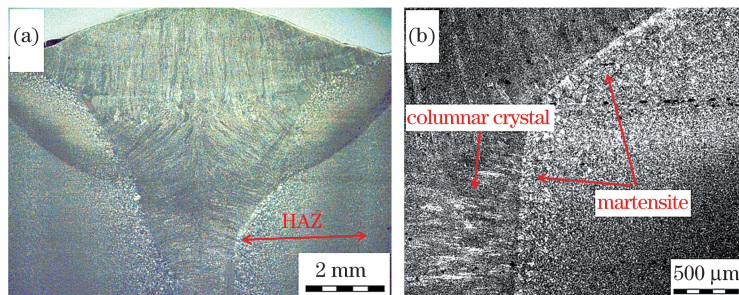


图7 B950CF高强钢的MAG焊接头。(a)宏观形貌;(b)金相组织

Fig. 7 MAG welded joint of B950CF steel. (a) Macro-morphology; (b) metallographic structure

Ultra-NGLW接头的微观组织较复杂,焊缝填充层中间和底部主要由针状铁素体和粒状贝氏体组成。形成这种组织的原因是,底部和中间的填充层在后来填充层的重熔和多次类似高温的回火热作用^[14]下,仍保留原来的马氏体取向[图8(c)、(d)],而分散在白色针状铁素体上的黑色

3 结果及讨论

3.1 Ultra-NGLW接头的微观组织

对比B950CF贝氏体高强钢的熔化极活性气体保护电弧(MAG)焊接头(图7)与Ultra-NGLW接头(图8),MAG焊接头的焊缝组织包含粗大的块状铁素体、低碳马氏体和柱状晶,焊缝组织从中间向熔合线方向生长,熔合线处有板条马氏体存在。

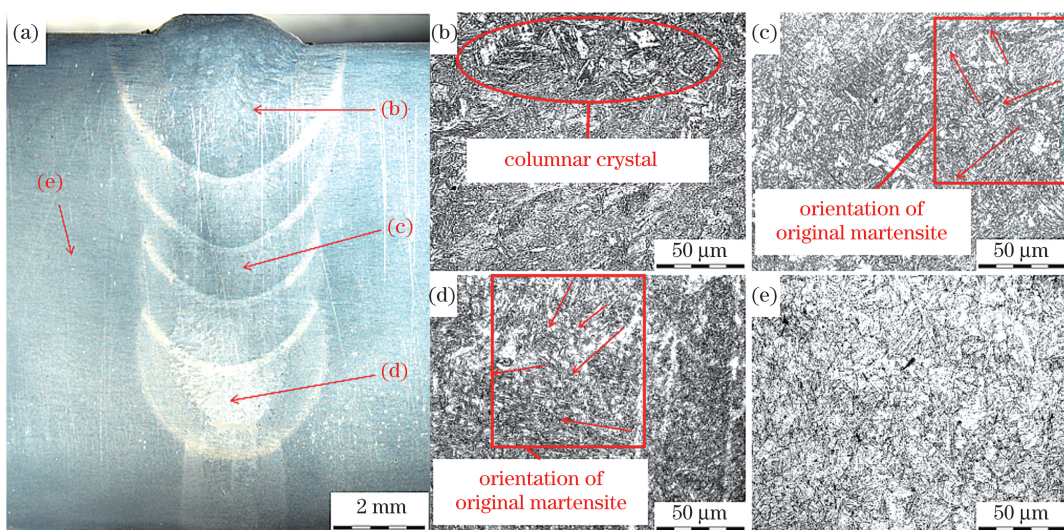


图8 Ultra-NGLW接头形貌。(a)接头焊缝宏观形貌;(b)盖面填充层组织;(c)第4填充层组织;(d)第2填充层组织;(e)母材组织

Fig. 8 Morphology of Ultra-NGLW joint. (a) Macro-morphology of joint weld; (b) microstructure of cover filling layer; (c) microstructure of 4th filling layer; (d) microstructure of 2nd filling layer; (e) microstructure of base material

3.2 微型剪切试验结果

与焊缝中心的距离设为 L 。从微型剪切试验结

色粒状贝氏体对接头的强度和韧性有增强作用^[15]。

表面填充层的组织主要为铁素体和上贝氏体,并伴有柱状晶和低碳马氏体[图8(b)]。该层仅经历了一次熔凝的热过程,没有经历类似回火作用,其晶粒比中间填充层的晶粒更粗大。

果可以看出,三个试样的剪切应力都呈单峰分布,可以推断整个接头的剪切应力会呈“M”型。在距离焊

缝中心 10.8 mm[图 9(a)]处, 剪切强度变得平稳, 此处已超出热影响区, 是母材区域, 在距离焊缝中心 18 mm 处微型剪切试验停止。

在熔合线处, 三个试样均存在宽度为 150~200 μm 的板条马氏体带[图 9(b)], 具有脆硬、剪切强

度高的特点, 最大剪切强度为 658.8 MPa, 这里也是接头残余应力取得最大值的地方。随着 L 的增加, 熔合线中的马氏体组织逐渐转变为正火区的细铁素体和粒状贝氏体[图 9(c)], 其抗剪强度降低到与母材强度相近的水平, 且接头残余应力分布也趋于稳定。

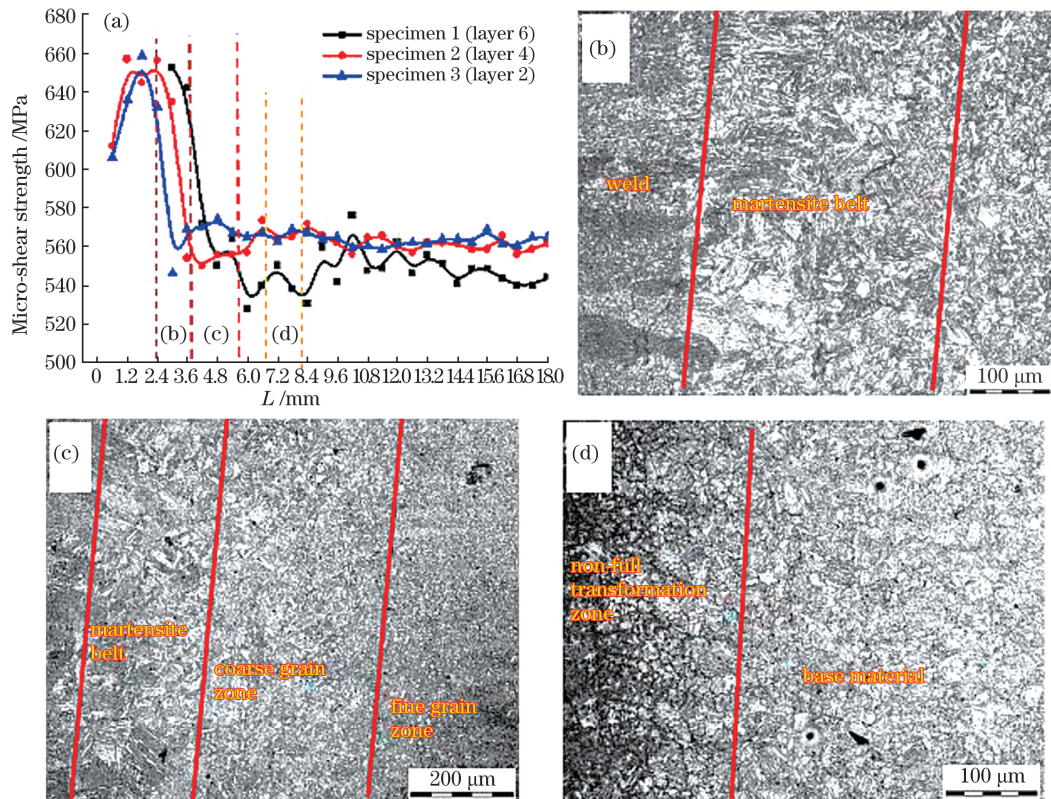


图 9 微型剪切强度结果及接头微观组织。(a)微型剪切强度与 L 的关系;(b)接头熔合线的微观组织;(c)热影响区的微观组织;(d)不完全相变区的微观组织

Fig. 9 Results of micro-shear strength and microstructures of joint. (a) Micro-shear strength versus L ; (b) microstructure of joint fusion line; (c) microstructure of HAZ; (d) microstructure of non-full phase-transformation zone

三组试样所表征的接头韧性如图 10(a)所示, 根据剪切强度和(5)式计算得到的接头的抗拉强度如图 10(b)所示。

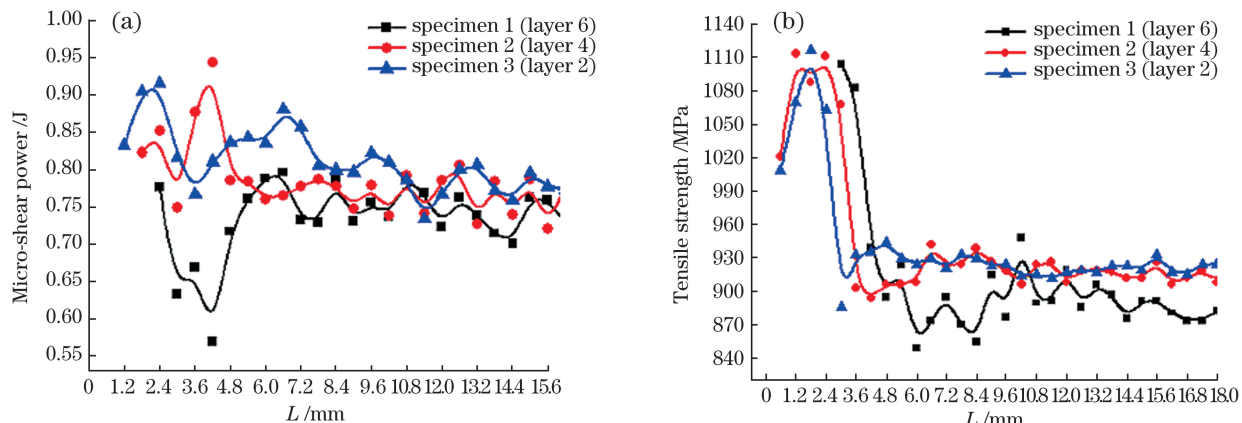


图 10 微型剪切试验得到的韧性和计算得到的抗拉强度。(a)微型剪切功;(b)抗拉强度与 L 的关系

Fig. 10 Toughness obtained by micro-shear test and calculated tensile strength. (a) Micro-shear power; (b) tensile strength versus L

通过计算接头微区的剪切功,可以看出,specimen 2 和 specimen 3 的最高韧性位于接头热影响区。specimen 3 的韧性略优于 specimen 2,这是因为后焊的焊缝填充层在焊接过程中对之前焊道反复的热作用,使之前的填充层产生类似回火,晶粒细化[图 8(c)和图 8(d)],从而韧性得到提高。而specimen 1 即盖面层,具有较低的韧性,特别是热影响区,这与中间和底部填充层的韧性特点正好相反。这是因为 specimen 1 是最后的填充层,不受重熔和类回火效应作用。从金相组织[图 8(b)]还发现,specimen 1 的焊缝组织粗大且呈片状,存在柱状晶

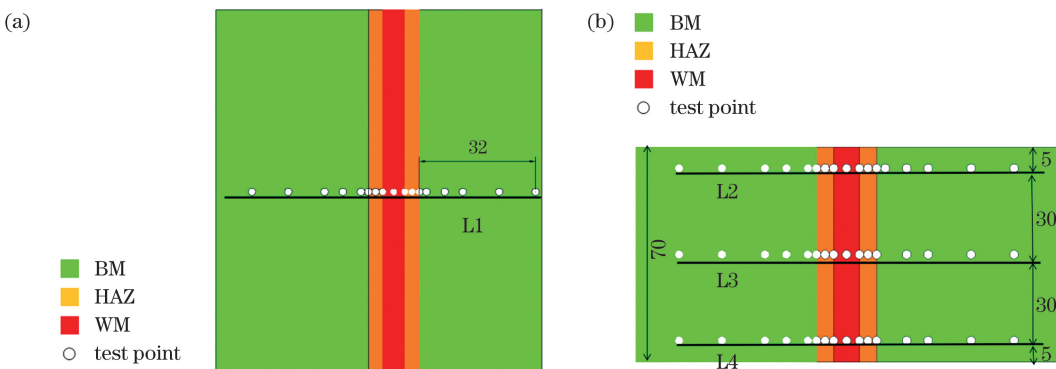


图 11 Ultra-NGLW 接头残余应力的测试布点。(a)L1 测试线;(b)L2、L3 和 L4 测试线

Fig.11 Residual stress test points for Ultra-NGLW joint. (a)L1 test line;(b)L2, L3 and L3 test lines

20 mm 接头上表面测试线(L1)的残余应力测试结果如图 12(a)所示。接头横向残余应力的整体分布呈“W”型:焊趾处(熔合线)为最大压应力点,焊缝中心处的压应力为-162 MPa,焊趾处的压应力最大值为-476 MPa。纵向残余应力为“M”型分布:热影响区有最大拉应力 170 MPa,焊缝和焊趾都为压应力状态。

50 mm 接头上表面测试线(L1)的残余应力测试结果如图 12(b)所示。与 20 mm 接头的分布相同,横向残余应力也呈“W”型:最大压应力(-400 MPa)点出现在焊趾处,焊缝中心处的压应力为-22 MPa。纵向残余应力分布同样也为“M”型分布:最大拉应力为 99 MPa。

70 mm 接头上表面测试线(L1)的残余应力测试结果如图 12(c)所示。与 20 mm 接头、50 mm 接头的残余应力分布一致,70 mm 接头的横向残余应力和纵向残余应力也是在熔合线处有最大压应力(-214 MPa),而热影响区的细晶区拉应力为最大值(166 MPa)。纵向残余应力呈现“M”型分布,热影响区的最大拉应力为 321 MPa。

对比三种不同厚度接头的表面残余应力,如

和低碳马氏体。然而,所有试样的韧性在熔合线处均陡降,这是由熔合线处的马氏体带引起的[图 9(b)]。

3.3 接头残余应力

图 11 为超窄间隙激光填丝焊接头的测试布点。考虑到焊缝和热影响区的宽度,在接头表面的焊缝中心、焊趾、热影响区、热影响区边缘以及母材区域对称布点(L1 测试线)。在厚度为 70 mm 的接头截面布置三条测试线,分别位于盖面填充层(L2 测试线)、中间填充层(L3 测试线)以及激光打底层(L4 测试线)。

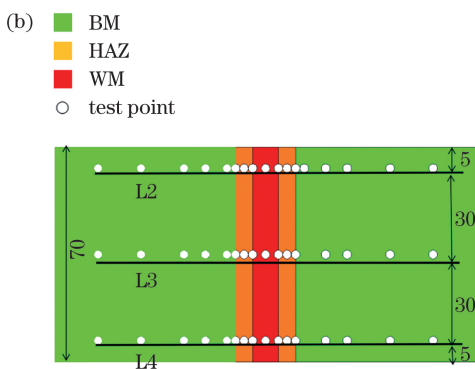


图 13 所示,其具有类似的分布:横向残余应力为“W”分布[图 13(b)],残余拉应力的峰值出现在焊缝中心和热影响区,而熔合线处的残余压应力最大;纵向应力均呈“M”型分布[图 13(c)]。从接头厚度对残余应力的影响来看,70 mm 接头的残余拉应力值高于 20 mm 和 50 mm 接头,横向残余拉应力最高值为 166 MPa,纵向残余拉应力最高值为 342 MPa。20 mm 接头的横向残余应力主要为压应力,最大拉应力仅为 43 MPa,50 mm 接头的残余应力大小与 20 mm 接头相近,最大残余拉应力为 155 MPa。因为厚度不同,在焊接过程中,接头的坡口收缩量和接头整体的累积形变量也会有所不同,所以接头表面应力出现差异。王桂兰等^[16]指出:随着基板厚度的增加,基板翘曲变形显著减小直至基本稳定;成形件第一主应力的应力区面积逐渐减小,成形件的纵向残余应力最大值略有波动但相对稳定。这证明熔池给不同厚度的厚板带来了不同变形,这些变形会影响表面的残余应力。除此之外,不同厚度接头的填丝焊接道层数不同,接头经历的热循环次数不同,这会导致接头整体残余应力的分布出现一定程度的差异,不同的应力分布可能导致表面残余应力变化。

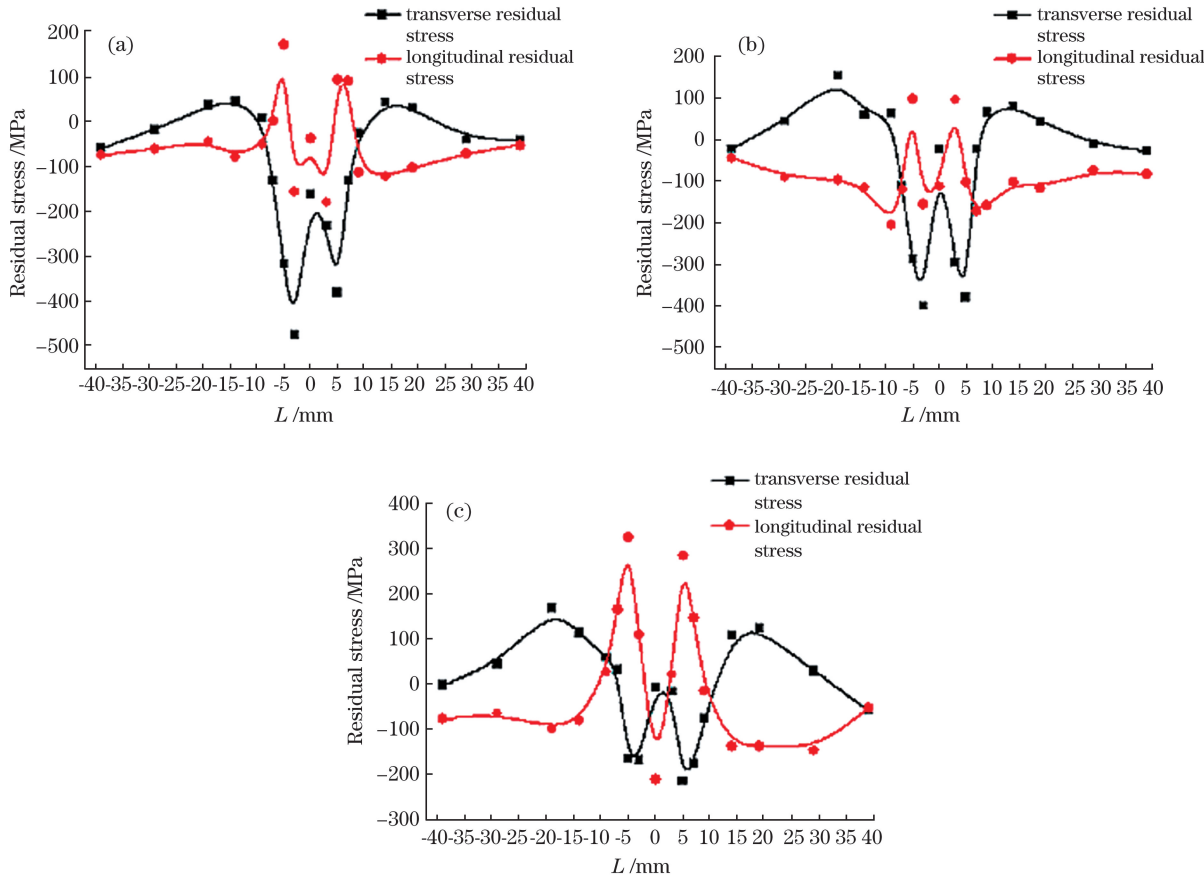


图 12 Ultra-NGLW 接头上表面残余应力的测试结果。(a)20 mm 接头;(b)50 mm 接头;(c)70 mm 接头

Fig. 12 Test results of upper surface residual stress of Ultra-NGLW joint. (a) 20 mm joint; (b) 50 mm joint; (c) 70 mm joint

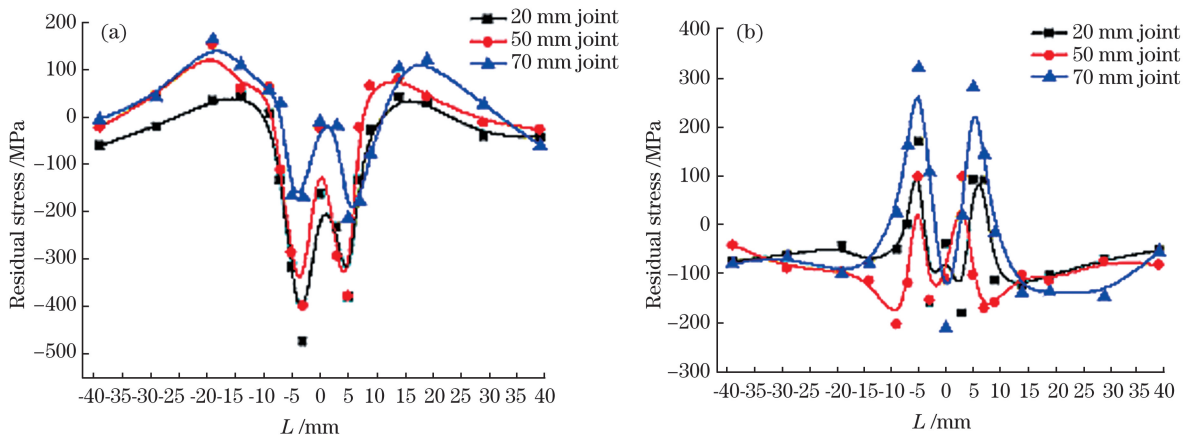


图 13 不同厚度 Ultra-NGLW 接头的残余应力比较。(a)横向残余应力;(b)纵向残余应力

Fig. 13 Residual stress comparison of Ultra-NGLW joints with different thicknesses. (a) Transverse residual stress; (b) longitudinal residual stress

图 14(a)是 70 mm 厚 Y 型坡口 Ultra-NGLW 接头截面残余应力的模拟计算结果。模拟计算得到的接头残余拉应力的最大值位于焊缝中心, 并没有出现在接头表面, 在填充层的 1~17 层均有大于 550 MPa 的残余拉应力, 焊缝中心的残余拉应力最大值为 662 MPa, 而实测的截面残余应力在

L2 处的最大值也有 362 MPa[图 14(b)]; 在模拟计算中, 熔合线处也出现残余压应力, 最大残余压应力值为 -364 MPa, 实测的表面残余应力在 L1 处为 -214 MPa, 实测的截面熔合线的最大残余压应力出现在中间填丝层(L3 测试线), 为 -358 MPa。

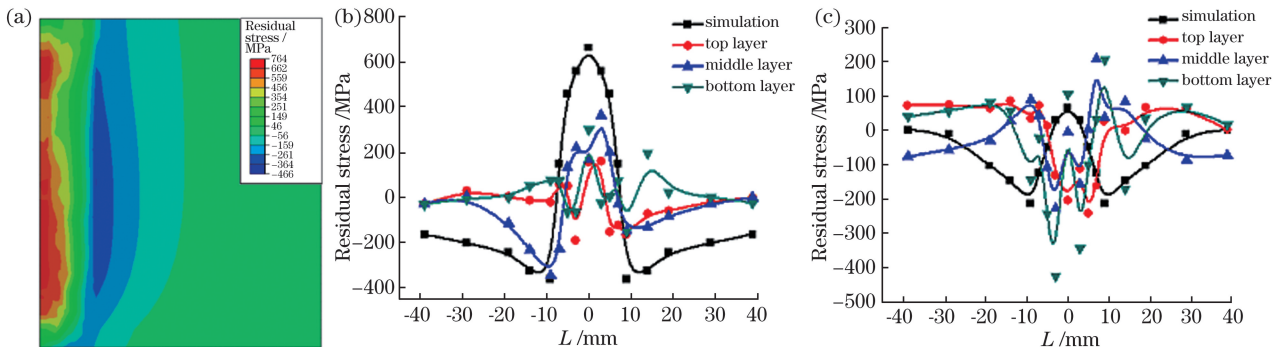


图 14 70 mm 厚接头的截面残余应力。(a) 数值模拟结果;(b) 横向残余应力;(c) 纵向残余应力

Fig. 14 Cross-sectional residual stress of 70 mm joint. (a) Numerical simulation result; (b) transverse residual stress; (c) longitudinal residual stress

葛森等^[17]指出,接头残余应力的最大值出现在焊缝表面下的 5~10 mm 处。其主要原因是填丝焊层对上一道焊层的重熔和高温回火作用使填丝焊层中的马氏体组织分解,焊缝在微观上表现为保留马氏体位向的针状铁素体,在宏观上则表现为接头焊缝的相对软化,马氏体分解带来的体积收缩使该处产生了较大的残余拉应力^[18-19]。但是 Ultra-NGLW 接头最后的盖面填充层并没有经历类似的重熔或者回火效应,马氏体得以保留,所以接头上表面的残余拉应力小于中间填充层,次表面的填充层有最大的残余拉应力。

张亮^[20]研究了中厚板激光多层焊温度场与应力应变场,也发现了这种接头应力“拉-压-拉”的分布特点,他指出中厚板激光多层焊焊缝内部存在“带状”应力集中,而预热能够有效缓解这种“带状”应力集中。通过对 Ultra-NGLW 接头微观组织的观察和微型剪切试验,发现压应力较大处的熔合区为板条马氏体,而在激光打底层和盖面填丝层有低碳马氏体和较粗大的块状铁素体,因此推测这种可以由预热工艺缓解的“带状”应力集中与接头中的马氏体有关。黄惠茹等^[21]指出,在低碳钢的热处理中,马氏体相变越多,体积膨胀越大,残余压应力值越高。可以推测,Ultra-NGLW 接头熔合线处产生的马氏体硬脆带导致该处出现较大的残余压应力,“打断”了残余应力分布的连续性。

4 结 论

通过对厚度分别为 20, 50, 70 mm 的焊接接头的表面残余应力进行测试,研究了焊接厚度对 Ultra-NGLW 接头表面残余应力的影响。通过模拟计算和实际测试相结合的方法,对厚度为 70 mm 的接头残余应力进行了分析和对比研究,并结合焊接

接头的微观组织,分析了微观组织对 Ultra-NGLW 接头残余应力分布的影响。研究结果证明,超窄间隙激光填丝焊在减小贝氏体钢厚板焊接的残余应力和变形方面有着较大优势。

参 考 文 献

- [1] Webster G A, Ezeilo A N. Residual stress distributions and their influence on fatigue lifetimes [J]. International Journal of Fatigue, 2001, 23: 375-383.
- [2] Li R Y, Wang T J, Wang C M, et al. A study of narrow gap laser welding for thick plates using the multi-layer and multi-pass method [J]. Optics & Laser Technology, 2014, 64: 172-183.
- [3] Li L Q, Zhang L, Dai J M. Numerical simulation of temperature and stress fields in wire filling laser multilayer welding [J]. Chinese Journal of Lasers, 2011, 38(10): 1003002.
- [4] Yang M. A finite element analysis of residual stress in heavy plate weldment [D]. Beijing: Beijing University of Technology, 2003.
- [5] Yin J, Li L Q, Tao W, et al. Weld microstructure characteristics of dual laser beam multi-layer welded high strength steel with filler wire [J]. Chinese Journal of Lasers, 2010, 37(5):1361-1367.
- [6] Shi Y, Fan D, Chen J H. Predication of properties of welded joints based on neural network [J]. Transactions of the China Welding Institution, 2004, 25(2): 73-76.

- 石坪, 樊丁, 陈剑虹. 基于神经网络方法的焊接接头力学性能预测[J]. 焊接学报, 2004, 25(2): 73-76.
- [7] Quan S Y, Lei B L. Application of the micro-shear test to selection of welding wires[J]. Materials for Mechanical Engineering, 2005, 29(5): 19-20, 60.
- 权思勇, 雷斌隆. 微型剪切试验在焊丝选择中的应用[J]. 机械工程材料, 2005, 29(5): 19-20, 60.
- [8] Zhang X P, Dorn L. Estimation of the local mechanical properties of pipeline steels and welded joints by use of the microshear test method [J]. International Journal of Pressure Vessels and Piping, 1998, 75(1): 37-42.
- [9] Lei B L, Wang Y L. Micro shear test and its use in welding technique[J]. Journal of Southwest Jiaotong University, 1990(1): 14-20.
- 雷斌隆, 王元良. 微型剪切试验法及基在焊接技术中的应用[J]. 西南交通大学学报, 1990(1): 14-20.
- [10] Wang J S, Hsieh C C, Lai H H, et al. The relationships between residual stress relaxation and texture development in AZ31 Mg alloys via the vibratory stress relief technique [J]. Materials Characterization, 2015, 99: 248-253.
- [11] Lin J, Ma N S, Lei Y P, et al. Measurement of residual stress in arc welded lap joints by cosa X-ray diffraction method [J]. Journal of Materials Processing Technology, 2017, 243: 387-394.
- [12] Diao L Y, Zhang C Z, Chen H, et al. Numerical simulation of narrow gap laser welding process of low alloy steel thick plate[J]. Hot Working Technology, 2019, 48(5): 199-202.
- 刁露阳, 张成竹, 陈辉, 等. 低合金钢厚板窄间隙激光焊接过程数值模拟[J]. 热加工工艺, 2019, 48(5): 199-202.
- [13] Zhang X P, Dorn L. Investigation on the possibility of using the microshear test as a surveillance method to estimate the mechanical properties and fracture toughness of nuclear pressure vessel steel, A508CL3, and its joints welded by narrow-gap submerged-arc welding[J]. International Journal of Pressure Vessels and Piping, 1999, 76(1): 35-41.
- [14] de Meester B. The weldability of modern structural TMCP steels[J]. ISIJ International, 1997, 37(6): 537-551.
- [15] Draugelates U, Schram A, Kolleck M. Significance of austenite grain size for transformation behaviour and toughness in the coarse-grain region of the heat-affected zone of fine-grain structural steels [J]. Schweissen & Schneiden, 1997, 49(5): E66-E69.
- [16] Wang G L, Mei F X, Zhang H O, et al. Influence of substrate thickness on stress field and warping deformation of substrate in arc deposition forming [J]. Hot Working Technology, 2017, 46(11): 181-184.
- 王桂兰, 梅飞翔, 张海鸥, 等. 基板厚度对电弧熔积成形应力场及基板翘曲变形的影响[J]. 热加工工艺, 2017, 46(11): 181-184.
- [17] Ge S. A method of measuring and computing triaxial residual stresses in thickness plate weldment [D]. Beijing: Beijing University of Technology, 2002.
- 葛森. 厚板焊接残余应力试验测量与计算[D]. 北京: 北京工业大学, 2002.
- [18] Ni C H, Guo G, Wu B X. Numerical analysis of welding stress and deformation of Q690 steel thick plates[J]. Hot Working Technology, 2019, 48(19): 160-163, 166.
- 倪川皓, 郭岗, 吴斌兴. Q690 钢厚板焊接应力变形的数值分析[J]. 热加工工艺, 2019, 48(19): 160-163, 166.
- [19] Dou L J. Test and analysis of temperature field and stress field of multi-layer multi-pass welding of Q345 thick plate [D]. Shenyang : Shenyang University of Technology, 2019.
- 窦丽杰. Q345 厚板多层多道焊温度场和应力场的测试分析[D]. 沈阳: 沈阳工业大学, 2019.
- [20] Zhang L. Numerical simulation of temperature and stress and strain fields in laser multilaye welding of mid-thick plate [D]. Harbin: Harbin Institute of Technology, 2011.
- 张亮. 中厚板激光多层焊温度场与应力应变场的数值模拟[D]. 哈尔滨: 哈尔滨工业大学, 2011.
- [21] Huang H R, Li X Y, Zhang L L, et al. Relationship among hardness, residual stress and microstructure of quenching low-carbon steel [J]. Science Technology and Engineering, 2017, 17(34): 191-196.
- 黄惠茹, 李晓阳, 张琳琳, 等. 淬火低碳钢硬度、残余应力和微观组织间的关系[J]. 科学技术与工程, 2017, 17(34): 191-196.

Effect of Microstructures of Ultranarrow Gap Laser Welded B950CF Steel Joints on Residual Stress Distribution

Zhang Chengzhu, Chen Hui*

Welding Research Institute, School of Materials Science and Engineering, Southwest Jiaotong University, Chengdu, Sichuan 610031, China

Abstract

Objective Ultra-narrow gap laser welding (ultra-NGLW) is a type of advanced welding technology for high-strength thick steel plates that use a laser as the heat source in an ultranarrow groove. It has the advantages of high welding accessibility and efficiency, low heat input and residual stress, and low deformation. Ultra-NGLW is suitable for welding thick high-strength steel plates in pressure vessels, ships, pipes, and hydropower equipment. Different from the common arc welded joints, in the process of multilayer filler wire welding, the complex thermal process differently changes the microstructure of each filling layer, resulting in different mechanical properties of each micro-zone. Therefore, the residual stress distribution in the ultranarrow gap laser welded high-strength steel joint is related to its special microstructure.

Methods In this paper, the B950CF bainitic high-strength steel and XK-01 wire with diameter of 1.2 mm were considered the research objects. Ultra-NGLW joints with three different thicknesses of 20, 50, and 70 mm were welded using the laser welding system comprising a TRUMPF-10002 high power laser and a Fronius automatic wire feeder.

Considering the complex microstructure and highly uneven mechanical properties of the ultra-NGLW joint, the micro-shear test was adopted to study the relationship between the mechanical properties and microstructures of the joint. The micro-shear specimen with a dimension of 1.5 mm × 1.5 mm × 40 mm, including weld metal (WM), heat-affected zone (HAZ), and base metal (BM), was cut from the different filling layers of the joint.

The surface residual stress of the joints with different thicknesses was measured using the μ X360n X-ray residual stress tester. Considering the variance of the thermal-physical and mechanical properties of the B950CF high-strength steel with temperature, the properties of the B950CF steel at different temperatures were calculated using the JMat Pro simulation software. Based on the ABAQUS simulation software, a simulation model of the 70-mm-thick ultraNGLW joint was established and the residual stress of this joint was calculated.

Results and Discussions The microstructure of the ultra-NGLW joint is considerably more complicated than that of the arc welded joint. The specimen 2 and specimen 3 mainly comprise acicular ferrite and granular bainite. Moreover, the microstructure of the cover layer mainly comprises ferrite and upper bainite, with a small amount of columnar crystals, and low-carbon martensite. The micro-shear test results indicate that the shear stress distribution of the three specimens is “M” type. Approximately 150–200 μ m lath martensite is observed at the fusion line, which is brittle and hard with high shear strength. The maximum shear strength is 658.8 MPa. It can be seen from the shear power in the micro-zone of the ultra-NGLW joint that the specimen 2 and specimen 3 exhibit the highest toughness, and the toughness of the cover layer is poor. The toughness of all specimens sharply decreases at the fusion line, which is attributed to the existence of martensite.

The residual stress of the ultra-NGLW joints is studied using X-ray nondestructive test and simulation. The results show that the residual stress distribution on the upper surface of the joints with different thicknesses is “W” shaped. The formation of martensite is the main reason for the high compressive stress (−214–−476 MPa) at the fusion line. The tensile stress increases with an increase in the joint thickness. The highest residual tensile stress (measured value of 362 MPa and calculated value of 662 MPa) is located in the weld subsurface filling layer. Because the martensite decomposes in the filling layer, the remelting and high temperature tempering cause the volume shrinkage and thus induce the large residual tensile stress. It interrupts the uniformity of the residual stress distribution.

Conclusions Results show that the specimen 2 and specimen 3 mainly comprise acicular ferrite and granular bainite. The micro-shear strength (600–630 MPa) is higher than that of the BM (570 MPa), and the weld fusion line

comprises lath martensite with the highest micro-shear strength of 658.8 MPa. The toughness of the middle and bottom filling layer is higher than that of the cover layer, which mainly comprises columnar crystals and low-carbon martensite.

The residual stress distribution on the upper surface of the ultra-NGLW joints with different thicknesses is “W” type. Owing to the existence of martensite, the compressive stress at the fusion line is -476 MPa (20 mm joint) and the highest tensile stress is 166 MPa (70 mm joint) in the fine-grain zone of HAZ. The tensile stress increases with an increase in the joint thickness.

The simulation results of the residual stress distribution of the 70-mm-thick ultra-NGLW joint matches the experimental results. The highest residual tensile stress (measured value of 362 MPa and calculated value of 662 MPa) is located in the weld subsurface filling layer. Because the martensite decomposes in the filling layer, the remelting and high temperature tempering cause the volume shrinkage and thus induce the large residual tensile stress.

Key words laser technique; ultra-narrow gap laser welding; residual stress; X-ray diffraction method; micro-shear test; high strength bainite steel

OCIS codes 140.3390;350.3390